Octant Degeneracy, Quadrant of CPV phase at Long Baseline ν Experiments and Baryogenesis

Kalpana Bora and Gayatri Ghosh
Department Of Physics, Gauhati University, Guwahati-781014, India

Debajyoti Dutta
Harish-Chandra Research Institute, Chhatnag Road, Jhunsi, Allahabad 211019, India

In a recent work by two of us, we have studied, how CP violation discovery potential can be improved at long baseline neutrino experiments (LBNE/DUNE), by combining with its ND (near detector) and reactor experiments. In this work, we discuss how this study can be further analysed to resolve entanglement of the quadrant of leptonic CPV phase and Octant of atmospheric mixing angle θ_{23}, at LBNEs. The study is done for both NH (Normal hierarchy) and IH (Inverted hierarchy), HO (Higher Octant) and LO (Lower Octant). We show how leptogenesis can enhance the effect of resolving this entanglement, and how possible values of the leptonic CPV phase can be predicted in this context. Carrying out numerical analysis based on the recent updated experimental results for neutrino mixing angles, we predict the values of the leptonic CPV phase for 152 possible cases. We also confront our predictions of the leptonic CPV phase with the updated global fit and find that five values of δ_{CP} are favoured by BAU constraints. One of the five values matches with the recent global fit value of δ_{CP} (leptonic CPV phase) close to 1.41π in our model independent scenario. A detailed analytic and numerical study of baryogenesis through leptogenesis is performed in this framework in a model independent way.

arXiv:1511.02452v2 [hep-ph] 4 Mar 2016

I. INTRODUCTION

Today, physics is going through precision era-this is more so for Neutrino physics. With the measurement of reactor angle θ_{13} [1–3] precisely by reactor experiments, the unknown quantities left to be measured in neutrino sector are – leptonic CP violating phase [4–9], octant of atmospheric angle θ_{23} [10–14], mass hierarchy, nature of neutrino etc. Long baseline neutrino experiments (LBNE [15, 16], NOνA [17] , T2K [18], MINOS [19], LBNO [20] etc) may be very promising, in measuring many of these sensitive parameters.

Exploring leptonic CP violation (CPV) is one of the most demanding tasks in future neutrino experiments [21]. The relatively large value of the reactor mixing angle θ_{13} measured with a high precision in neutrino experiments [22] has opened up a wide range of possibilities to examine CP violation in the lepton sector. The leptonic CPV phase can be induced by the PMNS neutrino mixing matrix [23] which holds, in addition to the three mixing angles, a Dirac type CP violating phase in general as it exists in the quark sector, and two extra phases if neutrinos are Majorana particles. Even if we do not yet have significant evidence for leptonic CPV, the current global fit to available neutrino data manifests nontrivial values of the Dirac-type CP phase [24, 25]. In this context, possible size of leptonic CP violation detectable through neutrino oscillations can be predicted. Recently, [4], two of us have explored possibiities of improving CP violation discovery potential of newly planned Long-Baseline Neutrino Experiments (earlier LBNE, now called DUNE) in USA. In neutrino oscillation probability expression $P(\nu_\mu \to \nu_e)$ relevant for LBNEs, the term due to significant matter effect, changes sign when oscillation is changed from neutrino to antineutrino mode, or vice-versa. Therefore in presence of matter effects, CPV effect is entangled and hence, one has two degenerate solutions - one due to CPV phase and another due to its entangled value. It has been suggested to resolve this issue by combining two experiments with different baselines [26, 27]. But CPV phase measurements depends on value of reactor angle θ_{13}, and hence precise measurement of θ_{13} plays crucial role in its CPV measurements. This fact was utilised recently

by two of us [4], where we explored different possibilities of improving CPV sensitivity for LBNE, USA. We did so by considering LBNE with
1. Its ND (near detector).
2. And reactor experiments.

We considered both appearance ($\nu_\mu \to \nu_e$) and disappearance ($\nu_\mu \to \nu_e$) channels in both neutrino and antineutrino modes. Some of the observations made in [4] are
1. CPV discovery potential of LBNE increases significantly when combined with near detector and reactor experiments.
2. CPV violation sensitivity is more in LO (lower octant) of atmospheric angle θ_{23}, for any assumed true hierarchy.
3. CPV sensitivity increases with mass of FD (far detector).
4. When NH is true hierarchy, adding data from reactors to LBNE improve its CPV sensitivity irrespective of octant.

Aim of this work is to critically analyse the results presented in [4], in context of entanglement of quadrant of CPV phase and octant of θ_{23}, and hence study the role of leptogenesis (and baryogenesis) in resolving this enganglement. Though in [4], we studied effect of both ND and reactor experiments on CPV sensitivity of the LBNEs, in this work we have considered only the effect of ND. But similar studies can also be done for the effect of Reactor experiments on LBNEs as well. The details of LBNE and ND are same as in [4]. Following the results of [4], either of the two octants is favoured, and the enhancement of CPV sensitivity with respect to its quadrant is utilized here to calculate the values of lepton-antilepton symmetry. This is done considering two cases of the rotation matrix for the fermions - CKM only, and CKM+PMNS. Then, this is used to calculate the value of BAU. This is an era of precision measurements in neutrino physics. We therefore consider variation of Δm^2_{31} within its 1σ, 2σ and 3σ range values. We calculate baryon to photon ratio, and compare with its experimentally known best fit value. We observe that the BAU can be explained most favourably for five possible cases explored here: IH, $\delta_{CP} = 1.43\pi$ and HO of θ_{23}; IH, $\delta_{CP} = 0.5277\pi$ and HO of θ_{23}; IH, $\delta_{CP} = 0.488\pi$ and LO of θ_{23}; IH, $\delta_{CP} = 0.383\pi$ and HO of θ_{23}; IH, $\delta_{CP} = 1.727\pi$ and LO of θ_{23}. It is worth mentioning that the value of $\delta_{CP} = 1.43\pi$ favoured by our calculation here is close to the central value of δ_{CP} from the recent global fit result [25, 28]. We also find that for variation of Δm^2_{31}, within its 1σ range, the calculated values of η_B for all possible five cases mentioned above lie in the allowed range of its best fit value. But for 3 σ variation of Δm^2_{31}, some of its values at its 3σ C.L are disfavoured. Also for the variation of θ_{13} within its 3 σ C.L, its values around 9.0974 are favoured, as far as matching with the best fit values of η_B are concerned. These results could be important keeping in view that the quadrant of leptonic CPV phase, and octant of atmospheric mixing angle θ_{23} are yet not fixed. Also, they are significant in context of precision measurements on neutrino oscillation parameters.

The paper is organized as follows. In Section II, we discuss entanglement of quadrant of CPV phase and octant of θ_{23}. In Section III, we present a review on leptogenesis and baryogenesis. In Sec. IV we show how the baryon asymmetry (BAU) within the SO(10) model, by using two distinct forms for the lepton CP asymmetry, can be used to break the entanglement. Sec. V summarizes the work.

II. CPV PHASE AND OCTANT OF θ_{23}

As discussed above, from Fig. 3 of [4], we find that by combining with ND and reactor experiments, CPV sensitivity of LBNE improves more for LO (lower octant) than HO (higher octant), for any assumed true hierarchy. In Fig. 1 below we plot CP asymmetry,

$$A_{CP} = \frac{P(\nu_\mu \to \nu_e) - P(\overline{\nu_\mu} \to \overline{\nu_e})}{P(\nu_\mu \to \nu_e) + P(\overline{\nu_\mu} \to \overline{\nu_e})} \tag{1}$$

as a function of leptonic CPV phase δ_{CP}, for $0 \leq \delta_{CP} \leq 2\pi$. It was shown in [4] that, using near detector (and combining with reactor experiments) at LBNE, the sentivity to measure CPV phase (and hence CP asymmetry) improves more at lower octant of θ_{23}. CP asymmetry also depends on the mass hierarchy. For NH, CP asymmetry is more in LO than in HO. For IH, CP asymmetry is more in LO than in HO. In this work we have used above information to calculate dependance of leptogenesis on octant of θ_{23} and quadrant of CPV phase. From Fig. 1 we see that

$$A_{CP}(LO) > A_{CP}(HO) \tag{2}$$

For a given true hierarchy, there are eight degenerate solutions

$$\delta_{CP}(\text{first quadrant}) - \theta_{23}(\text{lower octant})$$

$$\delta_{CP}(\text{second quadrant}) - \theta_{23}(\text{lower octant})$$

$$\delta_{CP}(\text{third quadrant}) - \theta_{23}(\text{lower octant})$$

$$\delta_{CP}(\text{fourth quadrant}) - \theta_{23}(\text{lower octant})$$

$$\delta_{CP}(\text{first quadrant}) - \theta_{23}(\text{higher octant})$$

$$\delta_{CP}(\text{second quadrant}) - \theta_{23}(\text{higher octant})$$

$$\delta_{CP}(\text{third quadrant}) - \theta_{23}(\text{higher octant})$$

$$\delta_{CP}(\text{fourth quadrant}) - \theta_{23}(\text{higher octant}) \tag{3}$$

This eight-fold degeneracy can be viewed as

$$\text{Quadrant of CPV phase} - \text{Octant of } \theta_{23} \tag{4}$$

entanglement. Out of these eight degenerate solutions, only one should be true solution. To pinpoint one true solution, this entanglement has to be broken. We have shown [4] that sensitivity to discovery potential of CPV at LBNEs in LO is improved more, if data from near detector of LBNEs, or from Reactor experiments is added to data from FD of LBNEs as shown in Fig. 3 of [4]. Therefore 8-fold degeneracy of (3) gets reduced to 4-fold degeneracy, with our

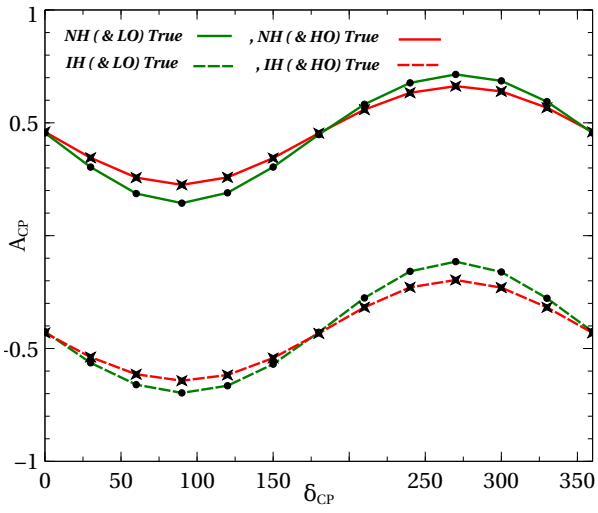

Figure 1: CP asymmetry vs δ_{CP} at DUNE/LBNE, for both the hierarchies. In Fig. 1 red and green solid (dotted) lines are for NH (IH) with types of curve to distinguish HO and LO as the true octant respectively.

proposal [4]. Hence, following this 4-fold degeneracy still remains to be resolved.

$$\delta_{CP}(\text{first quadrant}) - \theta_{23}(\text{LO})$$

$$\delta_{CP}(\text{second quadrant}) - \theta_{23}(\text{LO})$$

$$\delta_{CP}(\text{third quadrant}) - \theta_{23}(\text{LO})$$

$$\delta_{CP}(\text{fourth quadrant}) - \theta_{23}(\text{LO}) \tag{5}$$

The possibility of $\theta_{23} > 45^0$, ie HO of θ_{23} is also considered in this work. In this context the degeneracy is

$$\delta_{CP}(\text{first quadrant}) - \theta_{23}(\text{HO})$$

$$\delta_{CP}(\text{second quadrant}) - \theta_{23}(\text{HO})$$

$$\delta_{CP}(\text{third quadrant}) - \theta_{23}(\text{HO})$$

$$\delta_{CP}(\text{fourth quadrant}) - \theta_{23}(\text{HO}) \tag{6}$$

In this work, we propose that leptogenesis can be used to break above mentioned 4-fold degeneracy of Eq. (5),(6). It is known that observed baryon asymmetry of the Universe (BAU) can be explained via leptogenesis [29–33]. In leptogenesis, the lepton-antilepton asymmetry can be explained, if there are complex yukawa couplings or complex fermion mass matrices. This in turn arises due to complex leptonic CPV phases, δ_{CP}, in fermion mass matrices. If all other parameters except leptonic δ_{CP} phase in the formula for lepton - antilepton asymmetry are fixed, for example, then observed value of BAU from experimental observation can be used to constrain quadrant of δ_{CP}, and hence 4-fold entanglement of (5),(6) can be broken. An experimental signature of CP violation associated to the dirac phase δ_{CP}, in PMNS matrix [34], can in principle be obtained, by searching for CP asymmetry in ν flavor oscillation. To elucidate this proposal, we consider model independent scenario, in which BAU arises due to leptogenesis, and this

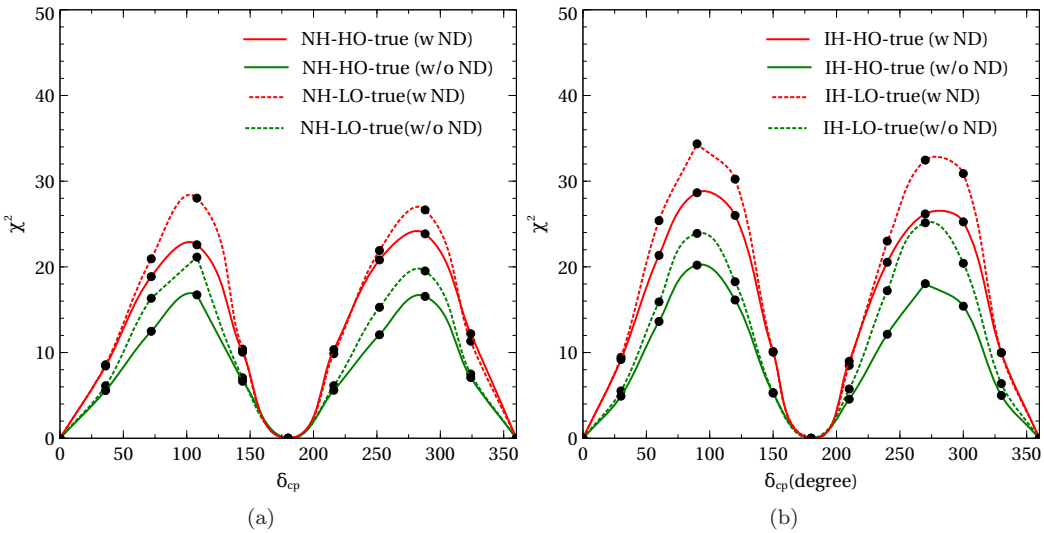

Figure 2: In Fig. 2a and 2b δ_{CP} Vs $\Delta\chi^2$ sensitivity corresponding to CP discovery potential at LBNEs, for both the hierarchies and octant is shown.

lepton-antilepton asymmetry [35] is generated by the out of equilibrium decay of the right handed, heavy majorana neutrinos, which form an integral part of seesaw mechanism for neutrino masses and mixings. Since our proposal is model independent, we consider type I seesaw mechanism, just for simplicity.

III. LEPTOGENESIS AND BARYOGENESIS IN TYPE I SEESAW SO(10) MODELS

In Grand Unified theories like SO(10), one right handed heavy majorana neutrino per generation is added to Standard Model [36–39], and they couple to left handed ν via Dirac mass matrix m_D. When the neutrino mass matrix is diagonalised, we get two eigen values − light neutrino $\sim \frac{m_D^2}{M_R}$ and a heavy neutrino state $\sim M_R$. This is called type I See Saw mechanism. Here, decay of the lightest of the three heavy RH majorana neutrinos, M_1, i.e $M_3, M_2 \gg M_1$ will contribute to $l-\bar{l}$ asymmetry (for leptogenesis), i.e ϵ_l^{CP}. In the basis where RH ν mass matrix is diagonal, the type I contribution to ϵ_l^{CP} is given by decay of M_1

$$\epsilon_l^{CP} = \frac{\Gamma(M_1 \to lH) - \Gamma(M_1 \to \bar{l}\bar{H})}{\Gamma(M_1 \to lH) + (\Gamma(M_1 \to \bar{l}\bar{H})}, \tag{7}$$

where $\Gamma(M_1 \to lH)$ means decay rate of heavy majorana RH ν of mass M_1 to a lepton and Higgs. We assume a normal mass hierarchy for heavy Majorana neutrinos. In this scenario the lightest of heavy Majorana neutrinos is in thermal equilibrium while the heavier neutrinos, M_2 and M_3, decay. Any asymmetry produced by the out of equilibrium decay of M_2 and M_3 will be washed away by the lepton number violating interactions mediated by M_1. Therefore, the final lepton-antilepton asymmetry is given only by the CP-violating decay of M_1 to standard model leptons (l) and Higgs (H). This contribution is [40]:

$$\epsilon_l = -\frac{3M_1}{8\pi}\frac{Im[\Delta m^2_{\odot} R^2_{12} + \Delta m^2_A R^2_{13}]}{v^2 \sum |R_{ij}|^2 m_j}. \tag{8}$$

R is a complex orthogonal matrix with the property that $RR^T = 1$. R can be parameterized as [41]:

$$R = D_{\sqrt{M^{-1}}} Y_\nu U D_{\sqrt{K^{-1}}}, \tag{9}$$

where Y_ν is the matrix of neutrino yukawa couplings. In the basis, where the charged-lepton Yukawa matrix, Y_e and gauge interactions are flavour-diagonal, $D_K = U^T K U$, where $K = Y_\nu^T M_R^{-1} Y_\nu$. U is the PMNS matrix and M_R is the RH neutrino Majorana scale. In the basis of right handed neutrinos, $D_M = Diag(M_1, M_2, M_3)$ where $M_3, M_2 \gg M_1$. Equation (8) relates the lepton asymmetry to both the solar (Δm^2_{21}) and atmospheric (Δm^2_A) mass squared differences. Thus the magnitude of the matter-antimatter asymmetry can be predicted in terms of low energy oscillation parameters, Δm^2_{21}, Δm^2_A and a CPV phase. Here matrix R is dependent on both U_{PMNS} and V_{CKM}, and it can be shown that,

$$\begin{aligned}
\mathrm{Im}R^2_{13} \;=\; & -\mathrm{Sin}(2\delta_q)\mathrm{Cos}^2(\theta^l_{23})\mathrm{Cos}^2(\theta^l_{13})\mathrm{Sin}^2(\theta^q_{13}) - 2\mathrm{Sin}(\delta_q)\mathrm{Cos}(\theta^q_{13})\mathrm{Cos}(\theta^l_{23})\mathrm{Cos}^2(\theta^l_{13})\mathrm{Sin}(\theta^q_{12})\mathrm{Sin}(\theta^q_{13})\mathrm{Sin}(\theta^l_{23}) \\
& +2\mathrm{Sin}(-\delta_l-\delta_q)\mathrm{Cos}(\theta^q_{12})\mathrm{Cos}(\theta^q_{13})\mathrm{Cos}(\theta^l_{23})\mathrm{Cos}(\theta^l_{13})\mathrm{Sin}(\theta^q_{13})\mathrm{Sin}(\theta^l_{13}) - 2\mathrm{Sin}(\delta_l)\mathrm{Cos}(\theta^q_{12})\mathrm{Cos}^2(\theta^q_{13})\mathrm{Cos}(\theta^l_{13}) \\
& \mathrm{Sin}(\theta^q_{12})\mathrm{Sin}(\theta^l_{23})\mathrm{Sin}(\theta^l_{13}) - \mathrm{Sin}(2\delta_l)\mathrm{Cos}^2(\theta^q_{12})\mathrm{Cos}^2(\theta^q_{13})\mathrm{Sin}^2(\theta^l_{13}) - 2\mathrm{Sin}(\delta_l)\mathrm{Cos}^2(\theta^q_{12})\mathrm{Cos}^2(\theta^q_{13})\mathrm{Sin}^2(\theta^l_{13})
\end{aligned}$$

$$\begin{aligned}
\mathrm{Im}R^2_{12} \;=\; & 2\mathrm{Sin}(\delta_q)\mathrm{Cos}(\theta^q_{13})\mathrm{Cos}^2(\theta^l_{12})\mathrm{Cos}(\theta^l_{23})\mathrm{Sin}(\theta^q_{12})\mathrm{Sin}(\theta^q_{13})\mathrm{Sin}(\theta^l_{23}) + 2\mathrm{Sin}(\delta_q)\mathrm{Cos}(\theta^q_{12})\mathrm{Cos}(\theta^q_{13})\mathrm{Cos}(\theta^l_{12})\mathrm{Cos}(\theta^l_{13}) \\
& \mathrm{Sin}(\theta^q_{13})\mathrm{Sin}(\theta^q_{12})\mathrm{Sin}(\theta^l_{23}) - \mathrm{Sin}(2\delta_q)\mathrm{Cos}^2(\theta^l_{12})\mathrm{Sin}^2(\theta^q_{13})\mathrm{Sin}^2(\theta^l_{23}) - 2\mathrm{Sin}(\delta_l-\delta_q)\mathrm{Cos}(\theta^q_{13})\mathrm{Cos}(\theta^l_{12})\mathrm{Cos}^2(\theta^l_{23}) \\
& \mathrm{Sin}(\theta^q_{12})\mathrm{Sin}(\theta^q_{13})\mathrm{Sin}(\theta^l_{12})\mathrm{Sin}(\theta^l_{13}) - 2\mathrm{Sin}(\delta_l-\delta_q)\mathrm{Cos}(\theta^q_{12})\mathrm{Cos}(\theta^q_{13})\mathrm{Cos}(\theta^l_{23})\mathrm{Cos}(\theta^l_{13})\mathrm{Sin}(\theta^q_{13})\mathrm{Sin}^2(\theta^l_{12})\mathrm{Sin}(\theta^l_{23}) \\
& -2\mathrm{Sin}(\delta_l)\mathrm{Cos}^2(\theta^q_{13})\mathrm{Cos}(\theta^l_{12})\mathrm{Cos}(\theta^l_{23})\mathrm{Sin}^2(\theta^q_{12})\mathrm{Sin}(\theta^l_{12})\mathrm{Sin}(\theta^l_{23})\mathrm{Sin}(\theta^l_{13}) + 2\mathrm{Sin}(\delta_l-2\delta_q)\mathrm{Cos}(\theta^l_{12})\mathrm{Cos}(\theta^l_{23}) \\
& \mathrm{Sin}^2(\theta^q_{13})\mathrm{Sin}(\theta^l_{12})\mathrm{Sin}(\theta^l_{23})\mathrm{Sin}(\theta^l_{13}) - 2\mathrm{Sin}(\delta_l)\mathrm{Cos}(\theta^q_{12})\mathrm{Cos}^2(\theta^q_{13})\mathrm{Cos}(\theta^l_{13})\mathrm{Sin}(\theta^q_{12})\mathrm{Sin}^2(\theta^l_{12})\mathrm{Sin}(\theta^l_{23})\mathrm{Sin}(\theta^l_{13}) \\
& +2\mathrm{Sin}(\delta_l-\delta_q)\mathrm{Cos}(\theta^q_{13})\mathrm{Cos}(\theta^l_{12})\mathrm{Sin}(\theta^q_{12})\mathrm{Sin}(\theta^q_{12})\mathrm{Sin}(\theta^l_{12})\mathrm{Sin}^2(\theta^l_{23})\mathrm{Sin}(\theta^l_{13}) + 2\mathrm{Sin}(2\delta_l-2\delta_q)\mathrm{Cos}^2(\theta^l_{23}) \\
& \mathrm{Sin}^2(\theta^q_{13})\mathrm{Sin}^2(\theta^l_{12})\mathrm{Sin}^2(\theta^l_{13}) + 2\mathrm{Sin}(2\delta_l-\delta_q)\mathrm{Cos}(\theta^q_{13})\mathrm{Cos}(\theta^l_{23})\mathrm{Sin}(\theta^q_{12})\mathrm{Sin}(\theta^q_{13})\mathrm{Sin}^2(\theta^l_{12})\mathrm{Sin}(\theta^l_{23})\mathrm{Sin}^2(\theta^l_{13}) \\
& +\mathrm{Sin}(2\delta_l)\mathrm{Cos}^2(\theta^q_{13})\mathrm{Sin}^2(\theta^q_{12})\mathrm{Sin}^2(\theta^l_{12})\mathrm{Sin}^2(\theta^l_{23})\mathrm{Sin}^2(\theta^l_{13})
\end{aligned}$$

$$R_{11} = \mathrm{Cos}(\theta^q_{12})\mathrm{Cos}(\theta^q_{13})\mathrm{Cos}(\theta^l_{12})\mathrm{Cos}(\theta^l_{13}) + e^{-i\delta_q}\mathrm{Sin}(\theta^q_{13})\mathrm{Sin}(\theta^l_{12})\mathrm{Sin}(\theta^l_{23}) - e^{-i\delta_l}e^{-i\delta_q}\mathrm{Sin}(\theta^q_{13})\mathrm{Cos}(\theta^l_{12})\mathrm{Cos}(\theta^l_{23})\mathrm{Sin}(\theta^l_{13})$$
$$-\mathrm{Cos}(\theta^q_{13})\mathrm{Sin}(\theta^q_{12})\mathrm{Cos}(\theta^l_{23})\mathrm{Sin}(\theta^l_{12}) - e^{-i\delta_l}\mathrm{Cos}(\theta^q_{13})\mathrm{Sin}(\theta^q_{12})\mathrm{Cos}(\theta^l_{12})\mathrm{Sin}(\theta^l_{23})\mathrm{Sin}(\theta^l_{13})$$

$$R_{12} = \mathrm{Cos}(\theta^q_{12})\mathrm{Cos}(\theta^q_{13})\mathrm{Cos}(\theta^l_{13})\mathrm{Sin}(\theta^l_{12}) - e^{-i\delta_q}\mathrm{Sin}(\theta^q_{13})\mathrm{Cos}(\theta^l_{12})\mathrm{Sin}(\theta^l_{23}) - e^{-i\delta_l}e^{-i\delta_q}\mathrm{Cos}(\theta^l_{23})\mathrm{Sin}(\theta^l_{12})\mathrm{sin}(\theta^l_{13})\mathrm{Sin}(\theta_{13}q)$$
$$-\mathrm{Cos}(\theta^q_{13})\mathrm{Sin}(\theta^q_{12})\mathrm{Cos}(\theta^l_{12})\mathrm{Cos}(\theta^l_{23}) - e^{-i\delta_l}\mathrm{Cos}(\theta^q_{13})\mathrm{Sin}(\theta^q_{12})\mathrm{Sin}(\theta^l_{12})\mathrm{Sin}(\theta^l_{23})\mathrm{Sin}(\theta^l_{13})$$

$$R_{13} = e^{-i\delta_q}\mathrm{Cos}(\theta^l_{23})\mathrm{Cos}(\theta^l_{13})\mathrm{Sin}(\theta^q_{13}) - \mathrm{Cos}(\theta^q_{13})\mathrm{Cos}(\theta^l_{13})\mathrm{Sin}(\theta^q_{12})\mathrm{Sin}(\theta^l_{23}) - e^{-i\delta_l}\mathrm{Cos}(\theta^q_{12})\mathrm{cos}(\theta^q_{13})\mathrm{Sin}(\theta^l_{13}) \quad (10)$$

where, θ^l_{23}, θ^l_{13}, θ^l_{12} denote the three ν mixing angles, θ^q_{23}, θ^q_{13}, θ^q_{12} are the quark mixing angles. δ_l and δ_q are the leptonic CPV phase and quark CPV phase respectively. When left-right symmetry is broken at high intermediate mass scale M_R in SO(10) theory, CP asymmetry is given by

$$\epsilon_l = -\frac{3M_1}{8\pi}\frac{Im[\Delta m^2_A R^2_{13}]}{v^2\sum|R_{ij}|^2 m_j} \quad (11)$$

where

$$|R_{11}|^2 = \mathrm{Cos}^2(\theta^l_{12})\mathrm{Cos}^2(\theta^l_{13}), |R_{12}|^2 = \mathrm{Sin}^2(\theta^l_{12})\mathrm{Cos}^2(\theta^l_{13}), |R_{13}|^2 = \mathrm{Cos}^2(\delta_l)\mathrm{Sin}^2(\theta^l_{13}) + \mathrm{Sin}^2(\delta_l)\mathrm{Sin}^2(\theta^l_{13})$$

and

$$\mathrm{Im}R^2_{13} = -\mathrm{Sin}^2(2\delta_l)\mathrm{Sin}^2(\theta^l_{13}) \quad (12)$$

The neutrino oscillation data used in our numerical calculations are summarised as follows [2].

$$\Delta m^2_{21}[10^{-5}eV^2] = 7.62 \pm 0.19$$

$$|\Delta m^2_{31}|[10^{-3}eV^2] = 2.55^{+0.06}_{-0.09}(2.43^{+0.07}_{-0.06})$$

$$\mathrm{Sin}^2\theta_{12} = 0.320^{+0.016}_{-0.017}$$

$$\mathrm{Sin}^2\theta_{23} = 0.613^{+0.022}_{-0.040}(0.600^{+0.026}_{-0.031})$$

$$\mathrm{Sin}^2\theta_{13} = 0.0246^{+0.0049}_{-0.0028}(0.0250^{+0.0026}_{-0.0027}) \quad (13)$$

For $\Delta m^2_{31}, Sin^2\theta_{23}, Sin^2\theta_{13}$, the quantities inside the bracket corresponds to inverted neutrino mass hierarchy and those outside the bracket corresponds to normal mass hierarchy. The errors are within the 1σ range of the ν oscillation parameters. It may be noted that some results on neutrino masses and mixings using updated values of running quark and lepton masses in SUSY SO(10) have also been presented in [42]. Though we consider 3-flavour neutrino scenario, 4-flavour neutrinos with sterile neutrinos as fourth flavour, are also possible [43]. It is worth mentionng that ν masses and mixings can lead to charged lepton flavor violation in grand unified theories like SO(10) [44].

The origin of the baryon asymmetry in the universe (baryogenesis) is a very interesting topic of current research. A well known mechanism is the baryogenesis via leptogenesis, where the out-of-equilibrium decays of heavy right-handed Majorana neutrinos produce a lepton asymmetry which is transformed into a baryon asymmetry by electroweak sphaleron processes [45–47]. Lepton asymmetry is partially converted to baryon asymmetry through B+L violating sphaleron interactions [48]. As proposed in [49], a baryon asymmetry can be generated from a lepton asymmetry. The baryon asymmetry is defined as:

$$Y_B = \frac{n_B - n_{\bar{B}}}{s} = \frac{n_B - n_{\bar{B}}}{7n_\gamma} = \frac{\eta_B}{7}, \quad (14)$$

where $n_B, n_{\bar{B}}, n_\gamma$ are number densities of baryons, antibaryons and photons respectively, s is the entropy density, η is the baryon-to-photon ratio, $5.7 \times 10^{-10} \leq \eta_B \leq 6.7 \times 10^{-10}$ (95 % C.L) [50]. The lepton number is converted into the baryon number through electroweak sphaleron process [45–47].

$$Y_B = \frac{a}{a-1} Y_L, a = \frac{8N_F + 4N_H}{22N_F + 13N_H}, \tag{15}$$

where N_f is the number of families and N_H is the number of light Higgs doublets. In case of SM, $N_f = 3$ and $N_H = 1$. The lepton asymmetry is as follows:

$$Y_L = d\frac{\epsilon_l}{g^*}. \tag{16}$$

d is a dilution factor and $g^* = 106.75$ in the standard case [49], is the effective number of degrees of freedom. The dilution factor d [49] is, $d = \frac{0.24}{k(lnk)^{0.6}}$ for $k \geq 10$ and $d = \frac{1}{2k}, d = 1$ for $1 \leq k \leq 10$ and $0 \leq k \leq 1$ respectively, where the parameter k [49] is, $k = \frac{M_P}{1.7\upsilon^2 32\pi\sqrt{g^*}} \frac{(M_D{}^\dagger M_D)_{11}}{M_1}$, here M_P is the Planck mass. We have used the form of Dirac neutrino mass matrix M_D from [51].

IV. ANALYSIS AND DISCUSSION OF RESULTS

For our numerical analysis, we take the current experimental data for three neutrino mixing angles as inputs, which are given at $1\sigma - 3\sigma$ C.L, as presented in [2]. Here, we perform numerical analysis and present results both for normal hierarchy, inverted hierarchy, HO, LO from Fig. 2. We have explored the CP asymmetry using Eq. (7)-Eq. (12) and corresponding baryon asymmetry using Eq. (14)-(16), for 152 different combinations (shown in Table I-XII) of the two hierarchies (NH and IH), two types of octants– LO and HO, w ND, w/o ND (with and without near detector) and δ_{CP} corresponding to maximum χ^2 (for maximum sensitivity from Fig. 2(a), 2(b)), for which the CP discovery potential of the DUNE is maximum. We also consider non maximal values of δ_{CP} corresponding to $\chi^2 = 4$, 9, 16, 25 from Fig. 2. We examine these different cases in the light of recent ratio of the baryon to photon density bounds, $5.7 \times 10^{-10} \leq \eta_B \leq 6.7 \times 10^{-10}$ (CMB), and checked for which of the 152 cases, our calculated value of $|\eta_B|$ lies within this range.

Case	**hierarchy, octant**	**w ND/ OR w/o ND**	δ_{CP}	ϵ_l	$\lvert\eta_B\rvert$
1	NH, LO	WND	101	$-.0000177532$	7.39703×10^{-8}
2	NH, LO	WND	280	$-.0000125002$	5.17312×10^{-8}
3	NH, LO	W/oND	108	$.0000153489$	6.35202×10^{-8}
4	NH, LO	W/oND	282	7.53352×10^{-6}	3.11769×10^{-8}
5	IH, LO	W/ND	83	2.56383×10^{-6}	1.06102×10^{-8}
6	IH, LO	W/ND	276	1.01403×10^{-6}	4.19647×10^{-9}
7	IH, LO	W/oND	88	1.46427×10^{-7}	6.05975×10^{-10}
8	IH, LO	W/oND	275	3.6845×10^{-6}	1.5248×10^{-8}

Table I: Calculated values of CP asymmetry ϵ_l and baryon to photon ratio $|\eta_B|$ in case of LO, for R_{1j} elements of R matrix consisting of U_{PMNS} and V_{CKM} for the values of δ_{CP} when the CP discovery potential of the LBNE/DUNE is maximum as shown in Fig. 2.

Case	hierarchy, Octant	w ND/ OR w/o ND	δ_{CP}	ϵ_l	$\lvert\eta_B\rvert$
1	NH, LO	WND	101	.0000268767	1.11227×10^{-7}
2	NH, LO	WND	280	.0000238272	9.86068×10^{-8}
3	NH, LO	W/oND	108	.0000231986	9.60055×10^{-8}
4	NH, LO	W/oND	282	.0000332106	1.3744×10^{-7}
5	IH, LO	WND	83	.0000109298	4.5232×10^{-8}
6	IH, LO	W/ND	276	-3.3319×10^{-6}	1.37888×10^{-8}
7	IH, LO	W/oND	88	2.96234×10^{-7}	1.22594×10^{-9}
8	IH, LO	W/oND	270	-9.18963×10^{-7}	3.80305×10^{-9}

Table II: Same as in Table I, except here R matrix consists of U_{PMNS} only.

We find that out of 32 different cases corresponding to maximal sensitivity χ^2 (from Fig. 2) as shown in Table I−IV, our calculated value of BAU is larger than the currently allowed range of BAU except for two cases: case 7 in table I and case 5 in table III for which the calculated $|\eta_B|$ is compatible with the present range of baryon to photon density ratio [50]. In Table I, case 7 which has $\delta_{CP} = 88^0$ or 0.488π (first quadrant), IH and atmospheric angle θ_{23} in LO has $\eta_B = 6.05975 \times 10^{-10}$, consistent with its best fit value, $\eta_B = 6.05 \times 10^{-10}$ [50]. For this case, $\epsilon_l = 1.46427 \times 10^{-7}$ lies within the Davidson and Ibbara bounds [39], ($\epsilon_l \leq 4.59 \times 10^{-5}$). In Table III, case 5 has $\delta_{CP} = 95^0$ or 0.5277π (second quadrant), IH and atmospheric angle θ_{23} in HO has BAU equal to 6.2157×10^{-10} which is in accord with the present $|\eta_B|$ bounds and it leads to CP asymmetry $|\epsilon_l| = 1.50195 \times 10^{-7}$ that lies within the Davidson and Ibarra bounds.

Figure 3 shows the allowed regions of $|\eta_B|$ in the plane charted by (Δm^2_{31}, $|\eta_B|$) for δ_{CP} allowed at maximal sensitivity of CP discovery potential from Fig. 2 (case 7 of Table I). Here we show the variation of $|\eta_B|$ with Δm^2_{31}, taking the variation of the later within its 1σ and 2σ limits. It can be seen that η_B for our calculation (blue solid line) lies within the result of its global fit value ($5.7 \times 10^{-10} < \eta_B < 6.7 \times 10^{-10}$) shown in [50].

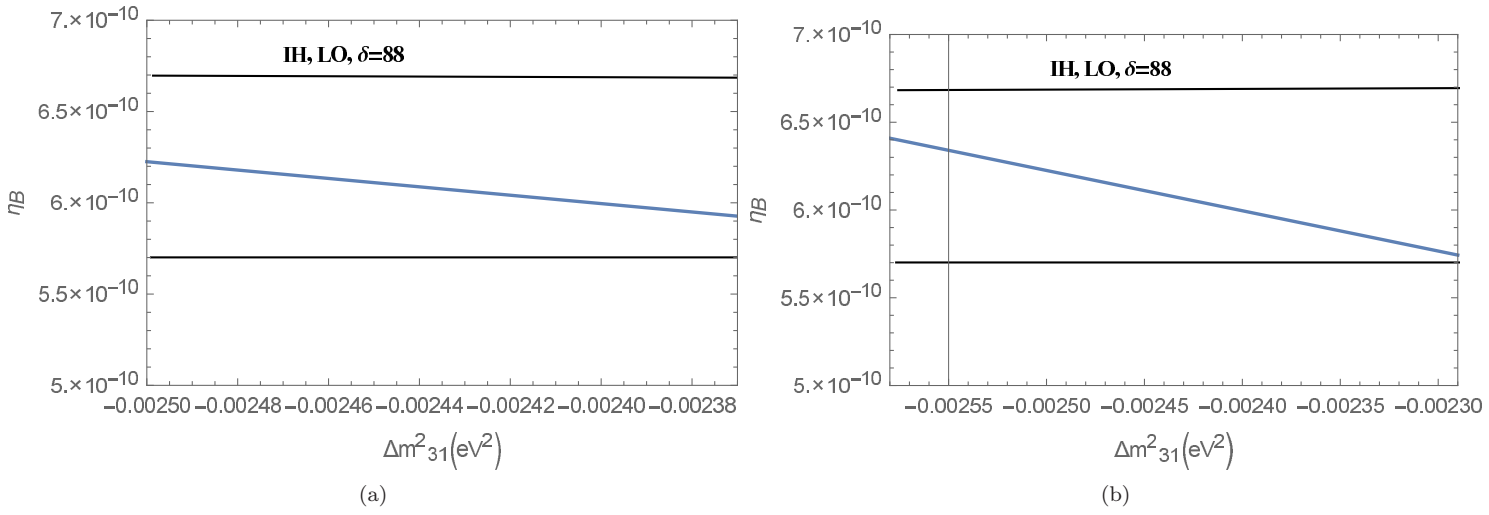

(a) (b)

Figure 3: Variation of η_B with Δm^2_{31}, for case 7 of Table I based on 1σ and 2σ range of Δm^2_{31} in Fig. 3(a) and 3(b) respectively. Plot of η_B Vs $\Delta m^2_{31}[eV^2]$ with CP phases $\delta_{CP} = 0.488\pi$ for the case when R matrix consists of both V_{CKM} and U_{PMNS}. The blue solid line in Fig. 3(a), 3(b) corresponds to θ_{23} in LO, $\delta_{CP} = 0.488\pi$ (first quadrant) and IH. The black horizontal line corresponds to the upper and lower limit on η_B, $5.7 \times 10^{-10} < \eta_B < 6.7 \times 10^{-10}$. As can be seen from the figure, the plots in Fig. 3(a), 3(b) satisfy the current experimental constraints on η_B.

Case	**hierarchy, octant**	**w ND/ w/o ND**	δ_{CP}	ϵ_l	$\lvert\eta_B\rvert$
1	NH, HO	WND	101	$-.0000189857$	7.85709×10^{-8}
2	NH, HO	WND	281	-3.51289×10^{-5}	1.45378×10^{-7}
3	NH, HO	W/oND	102	2.72017×10^{-5}	1.12572×10^{-7}
4	NH, HO	W/oND	283	-1.82461×10^{-5}	7.551×10^{-8}
5	IH, HO	W/ND	95	-1.50195×10^{-7}	6.2157×10^{-10}
6	IH, HO	W/oND	94	-8.7785×10^{-8}	3.63291×10^{-10}
7	IH, HO	W/ND	281	-5.8547×10^{-6}	2.42292×10^{-8}
8	IH, HO	W/oND	272	9.97129×10^{-6}	4.12654×10^{-8}

Table III: Same as in Table I, but HO values are used.

Case	**hierarchy, octant**	**w ND/ w/o ND**	δ_{CP}	ϵ_l	$\lvert\eta_B\rvert$
1	NH, HO	WND	101	.0000268767	1.11227×10^{-7}
2	NH, HO	WND	281	.0000112743	4.66576×10^{-8}
3	NH, HO	W/oND	102	6.73637×10^{-6}	2.78779×10^{-8}
4	NH, HO	W/oND	283	.0000163668	6.77325×10^{-8}
5	IH, HO	W/ND	95	4.1771×10^{-6}	1.72891×10^{-8}
6	IH, HO	W/oND	94	-1.99098×10^{-6}	8.23952×10^{-9}
7	IH, HO	W/ND	281	7.65022×10^{-6}	3.16598×10^{-8}
8	IH, HO	W/oND	272	$-.00001093$	4.52369×10^{-8}

Table IV: Same as in Table III, but R matrix consists of U_{PMNS} only.

Next, we explore values of δ_{CP} corresponding to $\chi^2 = 4$, 9, 16, 25 from Fig. 2 for which the CP discovery potential of the LBNE/DUNE is non maximal. For $\chi^2 = 2\ \sigma$, 3σ sensitivity of the CP discovery potential, Table V-VIII summarise the results where we find that out of the 64 possible cases in all, for 63 cases the calculated BAU is larger than the currently allowed range of BAU [50] by almost two to three orders of magnitude except for case 4 of Table VII where $\delta_{CP} = 1.924\ \pi$, IH, HO, has BAU of the order of 8.65034×10^{-12} less than the allowed $|\eta_B|$ limit.

We examine 56 possible cases for non maximal CP discovery sensitivity potential of the LBNE/DUNE from Fig. 2 summarised in Table IX-XII corresponding to χ^2 at 4σ, 5σ C.L out of which only 3 cases are consistent with the experimental results of $|\eta_B|$ bounds, (a) Case 15 of Table XI where $\frac{\delta_{CP}}{\pi} = 1.43$, ν mass spectrum of IH nature, atmospheric angle θ_{23} in HO, has CP asymmetry $\epsilon_l = 1.48671 \times 10^{-7}$ which lies within $|\epsilon_l^{max}| = 4.59 \times 10^{-5}$ (Davidson Ibbara bounds) and $|\eta_B| = 6.15262 \times 10^{-10}$ that agrees with the present BAU range. It is worth noting that this value of $\frac{\delta_{CP}}{\pi} = 1.43$ is close to the central value of δ_{CP} from the recent global fit result [28], (b) Case 13 of Table XI that locates $\frac{\delta_{CP}}{\pi} = 0.3833$, ν mass spectrum of IH nature, θ_{23} in HO, $\epsilon_l = 1.40342 \times 10^{-7}$ ($\leq |\epsilon_l^{max}| = 4.59 \times 10^{-5}$) has $|\eta_B| = 5.80973 \times 10^{-10}$, consistent with the allowed BAU range. Here R_{1j} elements of R matrix consists of U_{PMNS} and V_{CKM} in both the cases above, (c) Case 4 of Table XII which has $\frac{\delta_{CP}}{\pi} = 1.727$, IH ν mass spectrum, θ_{23} in LO, $|\epsilon_l| = 1.47958 \times 10^{-7}$ lies within $|\epsilon_l^{max}| = 4.59 \times 10^{-5}$ and $|\eta_B| = 6.12311 \times 10^{-10}$ that agrees with the current experimental constraints [50].

Case	hierarchy, Octant	$\Delta\chi^2$	δ_{CP}	ϵ_l	$\lvert\eta_B\rvert$
1	NH, LO	4	17	-3.57328×10^{-5}	1.4787×10^{-7}
2	NH, LO	9	38	1.91122×10^{-5}	7.90943×10^{-8}
3	NH, LO	9	147	3.19392×10^{-5}	1.32178×10^{-7}
4	NH, LO	4	154	3.33001×10^{-6}	1.3781×10^{-8}
5	NH, LO	4	203.5	3.31724×10^{-5}	1.37281×10^{-7}
6	NH, LO	9	213	1.18422×10^{-5}	4.9008×10^{-8}
7	NH, LO	9	332	-7.01565×10^{-6}	2.90337×10^{-8}
8	NH, LO	4	346.5	1.72854×10^{-6}	7.15341×10^{-9}
9	NH, HO	4	17	-3.6128×10^{-5}	1.49513×10^{-7}
10	NH, HO	4	155	-2.65416×10^{-5}	1.0984×10^{-7}
11	NH, HO	4	203	3.76207×10^{-5}	1.5569×10^{-7}
12	NH, HO	4	347.5	8.3309×10^{-7}	3.44768×10^{-9}
13	NH, HO	9	38.3	-1.54969×10^{-5}	6.41328×10^{-8}
14	NH, HO	9	147	3.09483×10^{-5}	1.28077×10^{-7}
15	NH, HO	9	212	-3.30145×10^{-5}	1.36628×10^{-7}
16	NH, HO	9	333.5	-1.97211×10^{-6}	8.16144×10^{-9}

Table V: Calculated values of CP asymmetry ϵ_l and baryon to photon ratio $|\eta_B|$ in case of NH, for R_{1j} elements of R matrix consisting of U_{PMNS} and V_{CKM} for DUNE/LBNE with its near detector, with $\chi^2 = 4$ and 9 measuring CP discovery sensitivity from Fig. 2.

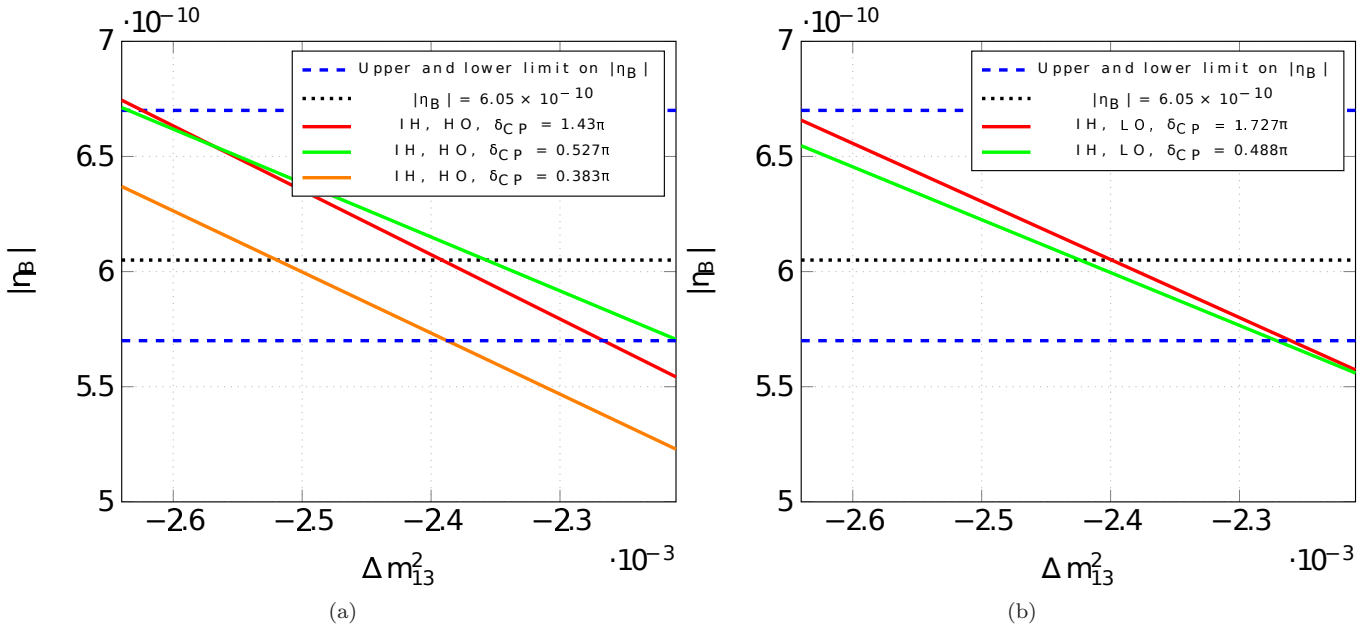

(a) (b)

Figure 4: Variation of η_B with Δm^2_{31} within its 3σ C.L. The upper and lower limit on η_B, $5.7 \times 10^{-10} < \eta_B < 6.7 \times 10^{-10}$ are characterised by blue dashed horizontal lines. Black dotted line corresponds to best fit value, $\eta_B = 6.05 \times 10^{-10}$. In the left panel, Fig. 4(a) shows the plot of η_B Vs Δm^2_{31} for $\delta_{CP} = 1.43\pi, 0.527\pi, 0.383\pi$. Fig. 4(b) of right panel frames the variation of η_B with Δm^2_{31} for $\delta_{CP} = 0.488\pi, 1.727\pi$.

Plugging the experimental data for Δm^2_{31} at 3σ C.L, and other ν oscillation parameters at best fit into Eq. (8 - 12) we predict the values of η_B from Eq. (14, 15, 16) as shown in the Fig. 4. The figure displays the allowed regions of $|\eta_B|$ in the plane $(\Delta m^2_{13}, |\eta_B|)$ for experimental results of Δm^2_{31} at 3σ C.L. In Fig. 4(a) red solid line conforms to the case 15 of Table XI, where $\delta_{CP} = 1.43\pi$, ν mass spectrum of IH structure, atmospherc angle θ_{23} in HO and $|\eta_B|$ in the range consistent with $5.7 \times 10^{-10} < \eta_B < 6.7 \times 10^{-10}$ except for $\Delta m^2_{31} > -2.2695 \times 10^{-3} eV^2$ and $\Delta m^2_{31} < -2.635 \times 10^{-3} eV^2$ where the red solid line departs from the experimental bound on η_B. The orange solid line in Fig. 4(a) depicts case 13 of Table XI which has $\delta_{CP} = 0.383\pi$, ν mass structure of IH spectrum, θ_{23} in HO and $|\eta_B|$ in the allowed range followed by the experimental constraints on $|\eta_B|$ except for $\Delta m^2_{31} > -2.385 \times 10^{-3} eV^2$. Slight variation of η_B for $\delta_{CP} = 0.5277\pi$ can be seen from Fig. 4(a) for $\Delta m^2_{31} < -2.63 \times 10^{-3} eV^2$ (green solid line). Similarly the green solid line in Fig. 4(b) corresponds to $\delta_{CP} = 0.488\pi$, IH ν spectrum, which is consistent with the allowed range of BAU for $\Delta m^2_{31} < -2.27 \times 10^{-3} eV^2$. The red solid line in Fig. 4(b) characterises case 4 of Table XII, which has $\delta_{CP} = 1.727\pi$, ν mass structure of IH nature, atmospherc angle θ_{23} in LO and $|\eta_B|$ in the range favoured by the present experimental limit on $|\eta_B|$, $5.7 \times 10^{-10} < |\eta_B| < 6.7 \times 10^{-10}$ except for $\Delta m^2_{31} > -2.255 \times 10^{-3} eV^2$ where the curve fails to fall in the allowed $|\eta_B|$ bounds even at 2σ C.L of Δm^2_{31}.

From the above discussion, we conclude that, out of total 152 cases presented in Table I-XII, only for five cases, the values of η_B lie within the experimental limits, which are summarised in Table XIII.

Case	**hierarchy, Octant**	$\Delta\chi^2$	δ_{CP}	ϵ_l	$\lvert\eta_B\rvert$
1	NH, LO	4	17	1.76335×10^{-5}	7.2975×10^{-8}
2	NH, LO	9	38	1.88675×10^{-5}	7.80817×10^{-8}
3	NH, LO	9	147	-3.2199×10^{-5}	1.33253×10^{-7}
4	NH, LO	4	203.5	-3.28826×10^{-6}	1.36082×10^{-7}
5	NH, LO	4	154	4.1195×10^{-6}	1.70482×10^{-8}
6	NH, LO	9	213	-3.16969×10^{-5}	1.31175×10^{-7}
7	NH, LO	9	332	-3.00567×10^{-5}	1.24385×10^{-7}
8	NH, LO	4	346.5	3.20414×10^{-5}	1.32601×10^{-7}
9	NH, HO	4	17	1.76335×10^{-5}	7.2975×10^{-8}
10	NH, HO	4	155	2.83588×10^{-5}	1.1736×10^{-7}
11	NH, HO	4	203	3.10849×10^{-5}	1.28642×10^{-7}
12	NH, HO	4	347.5	-2.16746×10^{-5}	8.96988×10^{-8}
13	NH, HO	9	38.3	3.10849×10^{-5}	1.28642×10^{-7}
14	NH, HO	9	147	-3.2199×10^{-5}	1.33253×10^{-7}
15	NH, HO	9	212	3.82461×10^{-6}	1.58278×10^{-8}
16	NH, HO	9	333.5	2.77229×10^{-7}	1.14729×10^{-7}

Table VI: Same as in Table V, but $R = U_{PMNS}$ only.

Figure 5 completes our discussion by showing the allowed regions in the plane $(\theta_{13}, |\eta_B|)$ which is done for five cases favoured by our analysis above. The shapes of the curves are somewhat symmetrical in Fig. 5(c) and 5(d) about $\theta_{13} = 9^0$ for $\delta_{CP} = 1.43\pi$, IH, θ_{23} in HO and $\delta_{CP} = 0.383\pi$, IH, θ_{23} in HO. For, $\delta_{CP} = 257.5^0$, values of θ_{13} around 9.0974^0 to 9.1^0, $9.2^0$to 9.22^0, 8.94^0 to 8.97^0, 8.82^0 to 8.84^0 are favoured which agrees well with the global fit value of θ_{13} [28]. For, $\delta_{CP} = 69^0$, values of θ_{13} around 9.0874^0 to 9.1^0, $9.21^0$to 9.2^0, 8.945^0 to 8.99^0 , 8.85^0 are favoured for

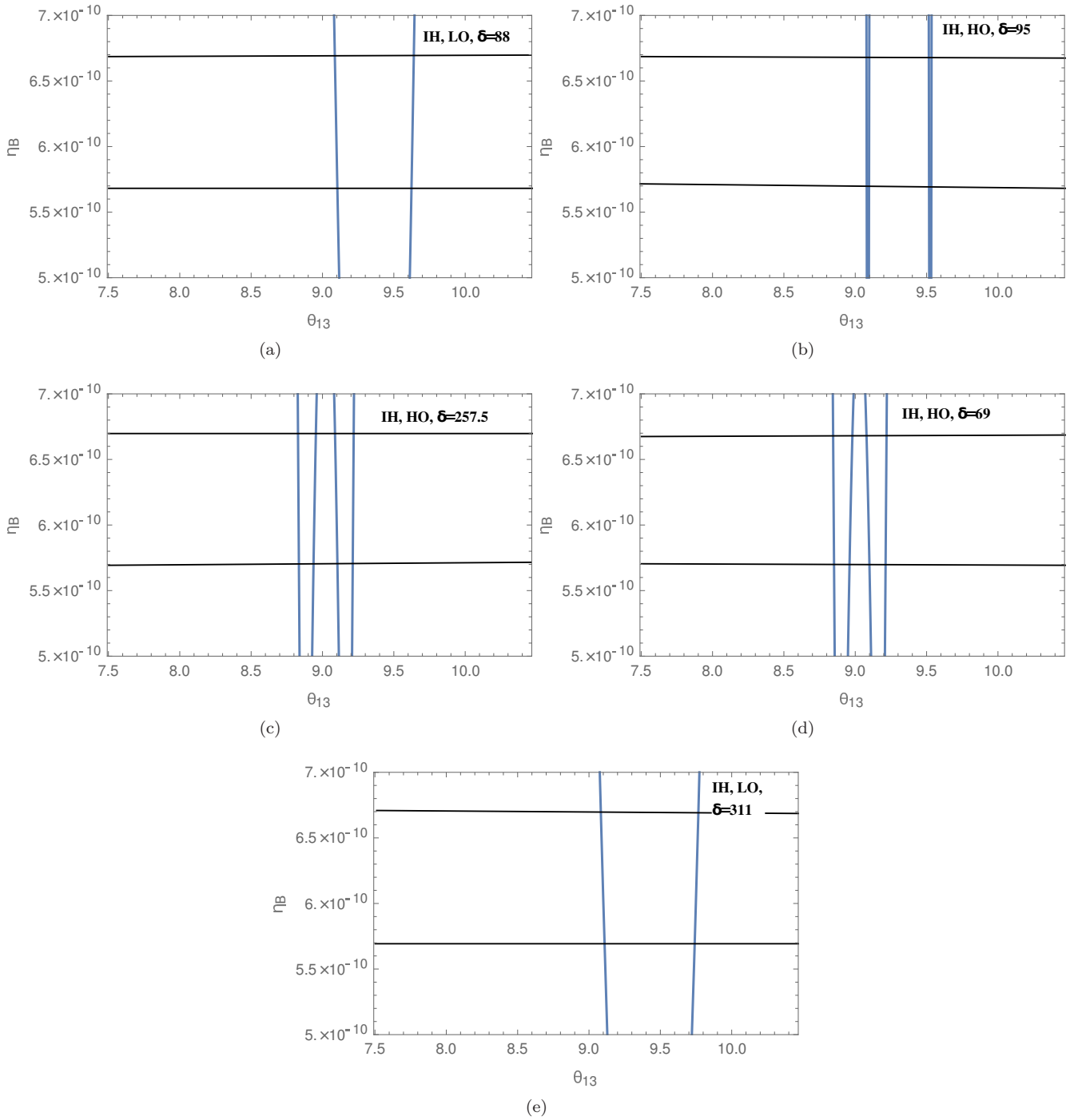

Figure 5: Plot of η_B vrs θ_{13} with CP phases in Fig. 5(a) $\delta_{CP} = 88^0$, IH, LO; in Fig. 5(b) $\delta_{CP} = 95^0$, IH, HO; in Fig. 5(c) $\delta_{CP} = 257.5^0$, IH, HO; in Fig. 5(d) $\delta_{CP} = 69^0$, IH, HO and in Fig. 5(e) $\delta_{CP} = 311^0$, IH, LO within the 3 σ errors of the best fit values of θ_{13} for the favoured cases. The black solid horizontal line corresponds to the upper and lower limit on η_B, $5.7 \times 10^{-10} < \eta_B < 6.7 \times 10^{-10}$.

$5.7 \times 10^{-10} < \eta_B < 6.7 \times 10^{-10}$ which is compatible with the global fit value of θ_{13} [28]. For, $\delta_{CP} = 88^0$ in Fig. 5(a), IH, θ_{23} in LO, values of θ_{13} around 9.0974^0 to 9.103^0, $9.61^0$to 9.65^0 are favoured for $5.7 \times 10^{-10} < \eta_B < 6.7 \times 10^{-10}$. Similarly for, $\delta_{CP} = 311^0$ in Fig. 5(e), IH, θ_{23} in LO, values of θ_{13} around 9.0974^0 to 9.12^0, $9.72^0$to 9.78^0 are mostly favoured for $5.7 \times 10^{-10} < \eta_B < 6.7 \times 10^{-10}$ which is consistent with the global fit data of θ_{13} at 2σ and 3σ C.L [28]. Lastly for $\delta_{CP} = 95^0$ in Fig. 5(b), IH, θ_{23} in HO, values of θ_{13} around 9.0974^0 to 9.11^0, $9.52^0$to 9.54^0 are mostly

favoured for $5.7 \times 10^{-10} < \eta_B < 6.7 \times 10^{-10}$ compatible with global fitting of θ_{13} at 2σ and 3σ C.L [28].

Case	**hierarchy, Octant**	$\Delta\chi^2$	δ_{CP}	ϵ_l	$\lvert\eta_B\rvert$
1	IH, HO	4	13.5	4.91465×10^{-6}	2.03389×10^{-8}
2	IH, HO	4	157.5	-7.63368×10^{-7}	3.15914×10^{-9}
3	IH, HO	4	202	1.24531×10^{-6}	5.15362×10^{-9}
4	IH, HO	4	346.3	-2.09025×10^{-9}	8.65034×10^{-12}
5	IH, HO	9	29	-5.98012×10^{-6}	2.47483×10^{-8}
6	IH, HO	9	153	1.18773×10^{-5}	4.91533×10^{-8}
7	IH, HO	9	209	8.38787×10^{-6}	3.47125×10^{-8}
8	IH, HO	9	332.5	2.45147×10^{-7}	1.01449×10^{-9}
9	IH, LO	9	332.5	1.03435×10^{-6}	4.28058×10^{-9}
10	IH, LO	9	209	5.36981×10^{-6}	2.22225×10^{-8}
11	IH, LO	9	153	7.94367×10^{-6}	3.28743×10^{-8}
12	IH, LO	9	29	-7.28224×10^{-6}	3.0137×10^{-8}
13	IH, LO	4	346.1	-1.04874×10^{-6}	4.34013×10^{-9}
14	IH, LO	4	203	1.26601×10^{-5}	5.23928×10^{-8}
15	IH, LO	4	157.5	-9.9942×10^{-7}	4.13602×10^{-9}
16	IH, LO	4	13.5	-3.75736×10^{-7}	1.55496×10^{-9}

Table VII: Same as in Table V, but IH is used.

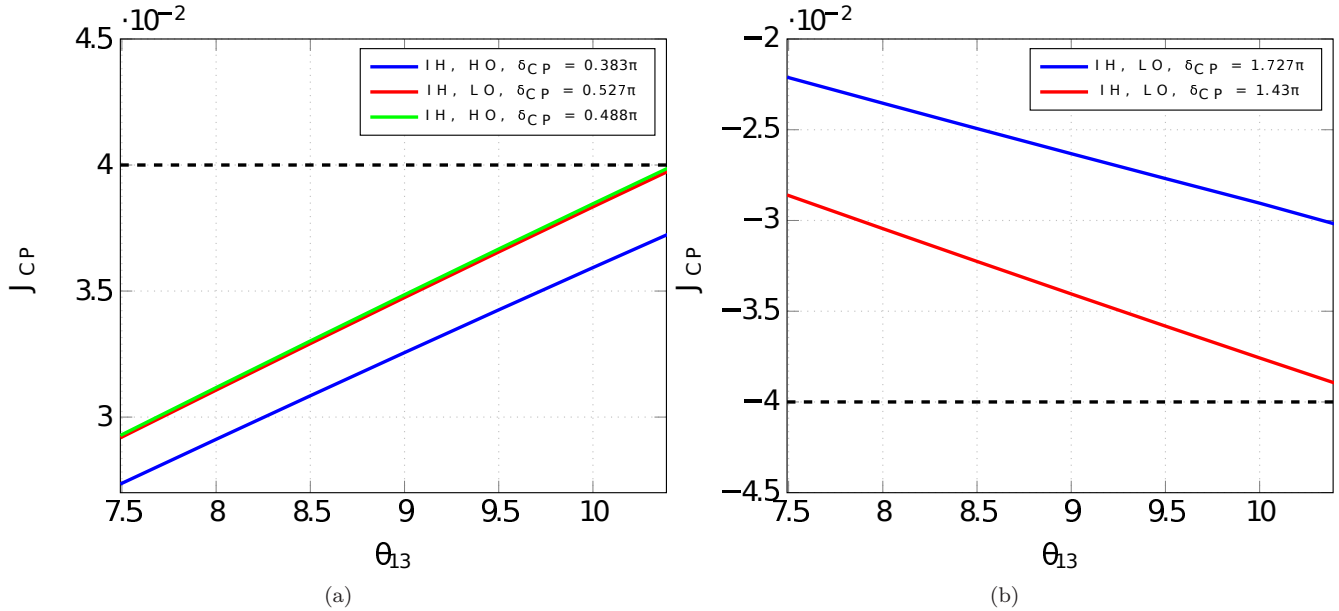

(a) (b)

Figure 6: Plot of J_{CP} vrs θ_{13} with CP phases in Fig. 6(a):$\delta_{CP} = 95^0$, IH, HO; $\delta_{CP} = 69^0$, IH, HO; $\delta_{CP} = 88^0$, IH, LO. Fig. 6(b): $\delta_{CP} = 257.5^0$, IH, HO; $\delta_{CP} = 311^0$, IH, LO within the 3 σ C.L of the best fit values of θ_{13}. Horizontal line represents the maximum allowed CP violation in the leptonic sector, $J_{CP} \leq .04|Sin\delta_{CP}|$.

The magnitude of CP violation in $\nu_l \to \nu_{l'}$ and $\nu_{\bar{l}} \to \nu_{\bar{l}'}$, $l = l^{'} = e, \mu, \tau$, is determined by the rephasing Jarkslog invariant J_{CP}, which in the standard parametrisation of the ν mixing matrix has the form [28]:

$$J_{CP} = Im(U_{\mu 3} U^*_{e3} U_{e2} U^*_{\mu 2}) = \frac{1}{8} Cos\theta_{13} Sin2\theta_{12} Sin2\theta_{23} Sin2\theta_{13} Sin\delta_{CP} \tag{17}$$

Since $Sin2\theta_{12}$, $Sin2\theta_{23}$, $Sin2\theta_{13}$ have been determined experimentally with a relatively good precision [1–3], the size of CP violation effects in ν oscillations depends essentially on leptonic CPV phase δ_{CP}. The current data implies $J_{CP} = 0.040|Sin\delta_{CP}|$ [28], and a best fit value J^{best}_{CP} = -0.032 [28]. Our calculated values of Jarkslog invariant by plugging input for the three ν mixing angles at its best fit for favoured cases of BAU and the values of leptonic δ_{CP} phase are summarised in Table XIII. We find that for all the five favoured cases, our calculated values of J_{CP} lie within its present experimental limits.

In Fig. 6 we plot J_{CP} Vs θ_{13}, taking variation of θ_{13} within 3σ range of its best fit value and find that the plot for all the above listed five cases, J_{CP} lies within its present experimental limits.

Case	**hierarchy, Octant**	$\Delta\chi^2$	δ_{CP}	ϵ_l	$\lvert\eta_B\rvert$
1	IH, HO	4	13.5	4.00427×10^{-6}	1.65714×10^{-8}
2	IH, HO	4	157.5	3.11981×10^{-6}	1.29111×10^{-8}
3	IH, HO	4	202	3.99325×10^{-6}	1.65258×10^{-8}
4	IH, HO	4	346.3	4.15622×10^{-6}	1.72002×10^{-8}
5	IH, HO	9	29	4.15708×10^{-6}	1.72038×10^{-8}
6	IH, HO	9	153	-3.99333×10^{-6}	1.65267×10^{-8}
7	IH, HO	9	209	-7.0083×10^{-7}	2.90033×10^{-9}
8	IH, HO	9	332.5	-3.56253×10^{-6}	1.47433×10^{-8}
9	IH, LO	9	332.5	1.03435×10^{-6}	4.28058×10^{-9}
10	IH, LO	9	209	-7.0083×10^{-7}	2.90033×10^{-9}
11	IH, LO	9	153	-3.99333×10^{-6}	1.65261×10^{-8}
12	IH, LO	9	29	4.15708×10^{-6}	1.72038×10^{-8}
13	IH, LO	4	346.1	3.63103×10^{-6}	1.50267×10^{-8}
14	IH, LO	4	203	-2.80629×10^{-6}	1.16136×10^{-8}
15	IH, LO	4	157.5	3.11981×10^{-6}	1.29111×10^{-8}
16	IH, LO	4	13.5	4.000427×10^{-6}	1.65714×10^{-8}

Table VIII: Same as in Table VI, but IH is used.

V. CONCLUSION

Measuring CP violation in the lepton sector is one of the most challenging tasks today. A systematic study of the CP sensitivity of the current and upcoming LBNE/DUNE is done in our earlier work [4] which may help a precision measurement of leptonic δ_{CP} phase. In this work, we studied how the entanglement of the quadrant of leptonic CPV phase and octant of atmospheric mixing angle θ_{23} at LBNE/DUNE, can be broken via leptogenesis and baryogenesis. Here, we have considered the effect of ND only in LBNE, on sensitivity of CPV phase measurement, but similar conclusions would hold for the effect of reactor experiments as well. This study is done for both Normal hierarchy and

Inverted hierarchy, Higher Octant and Lower Octant. We considered two cases of fermion rotation matrix - PMNS only, and CKM+PMNS. Following the results of [4], the enhancement of CPV sensitivity with respect to its quadrant is utilized here to calculate the values of lepton-antilepton symmetry. Then, this is used to calculate the value of BAU. This is an era of precision measurements in neutrino physics. We therefore considered variation of Δm^2_{31} within its 1σ, 2σ and 3σ, and θ_{13} within its 3σ range. We calculated baryon to photon ratio, and compared with its experimentally known best fit value.

Case	**hierarchy, Octant**	$\Delta\chi^2$	δ_{CP}	ϵ_l	$\lvert\eta_B\rvert$
1	NH, LO	16	56	1.35794×10^{-5}	5.62719×10^{-8}
2	NH, LO	16	136	-3.11475×10^{-5}	1.28902×10^{-7}
3	NH, LO	16	232	1.37456×10^{-5}	5.68851×10^{-8}
4	NH, LO	16	314	1.49244×10^{-6}	6.17636×10^{-9}
5	NH, LO	25	84	3.56574×10^{-5}	1.47565×10^{-7}
6	NH, LO	25	122.5	7.31569×10^{-6}	3.02754×10^{-8}
7	NH, LO	25	263.5	-1.25402×10^{-5}	5.18967×10^{-8}
8	NH, LO	25	294.5	4.28344×10^{-6}	1.77267×10^{-8}
9	NH, HO	16	59	3.19255×10^{-5}	1.32121×10^{-7}
10	NH, HO	16	132.5	-1.70443×10^{-5}	7.05367×10^{-8}
11	NH, HO	16	232.25	8.92875×10^{-6}	3.69509×10^{-8}
12	NH, HO	16	314	4.8229×10^{-6}	1.99592×10^{-8}

Table IX: Same as in Table V, but for $\chi^2 = 16$ and 25

Case	**hierarchy, Octant**	$\Delta\chi^2$	δ_{CP}	ϵ_l	$\lvert\eta_B\rvert$
1	NH, LO	16	56	-2.96623×10^{-5}	1.2275×10^{-7}
2	NH, LO	16	136	3.22739×10^{-5}	1.33563×10^{-7}
3	NH, LO	16	232	-2.72203×10^{-5}	1.12649×10^{-7}
4	NH, LO	16	314	-1.04375×10^{-5}	4.31949×10^{-8}
5	NH, LO	25	84	-3.32343×10^{-5}	1.37537×10^{-7}
6	NH, LO	25	122.5	-1.47354×10^{-6}	6.09812×10^{-9}
7	NH, LO	25	263.5	-2.36179×10^{-5}	9.77404×10^{-8}
8	NH, LO	25	294.5	-3.32892×10^{-6}	1.37765×10^{-7}
9	NH, HO	16	59	-3.27271×10^{-5}	1.35438×10^{-7}
10	NH, HO	16	132.5	-2.97961×10^{-5}	1.23309×10^{-7}
11	NH, HO	16	232.25	-1.46679×10^{-5}	6.07021×10^{-8}
12	NH, HO	16	314	-1.04375×10^{-5}	4.31949×10^{-8}

Table X: Same as in Table VI, but for $\chi^2 = 16$ and 25

To break the quadrant of CPV phase − Octant of θ_{23} entanglement we have calculated BAU (η_B) for 152 cases as shown in Tables I-XII, and found that only for five cases, our calculated η_B lies within the present best fit values of η_B.

These five cases are $\delta_{CP} = 1.43\pi$ (third quadrant), $\delta_{CP} = 0.527\pi$ (second quadrant), $\delta_{CP} = .383\pi$ (first quadrant), $\delta_{CP} = .488\pi$ (first quadrant) for the case when R matrix consists of both V_{CKM} and U_{PMNS} and $\delta_{CP} = 1.727\pi$ (fourth quadrant), for the case when R matrix consists of U_{PMNS} only. Next, we studied variation of η_B, w.r.t 1σ, 2σ and 3σ variation of Δm^2_{31}, as shown in Figs. 3 and 4. It can be seen from Fig. 3 and 4 that for variation of Δm^2_{31}, within its 1σ range, all calculated values of η_B lie in the allowed range of its best value. For Δm^2_{31} at its 3 σ C.L, the case $\delta_{CP} = 0.488\pi$ is consistent with the allowed range of BAU for $\Delta m^2_{31} < -2.27 \times 10^{-3} eV^2$. Similarly, very slight discrepancy of η_B for $\delta_{CP} = 0.5277\pi$ can be seen from Fig. 4(a) for $\Delta m^2_{31} < -2.63 \times 10^{-3} eV^2$. Case 15 of Table XI, where $\delta_{CP} = 1.43\pi$ has $|\eta_B|$ in the range compatible with $5.7 \times 10^{-10} < \eta_B < 6.7 \times 10^{-10}$ except for $\Delta m^2_{31} > -2.2695 \times 10^{-3} eV^2$ and $\Delta m^2_{31} < -2.635 \times 10^{-3} eV^2$. It is worth noting that this value of $\frac{\delta_{CP}}{\pi} = 1.43$ is close to the central value of δ_{CP} from the recent global fit result [28]. Case 13 of Table XI: $\delta_{CP} = 0.383\pi$ has $|\eta_B|$ in the range allowed by, $5.7 \times 10^{-10} < \eta_B < 6.7 \times 10^{-10}$ except for $\Delta m^2_{31} > -2.385 \times 10^{-3} eV^2$. Case 4 of Table XII, where $\delta_{CP} = 1.727\pi$, has $|\eta_B|$ in the range favoured by the present experimental constraints except for $\Delta m^2_{31} > -2.255 \times 10^{-3} eV^2$ where the straight line fails to satisfy allowed $|\eta_B|$ bounds even at 2σ C.L of Δm^2_{31}. Interestingly here leptonic CPV phase $\delta_{CP} = 1.727\pi$ lies within the 1σ ranges of δ_{CP} from latest global fit analysis, $\delta_{CP} = 1.67^{+0.37}_{-0.77}$ [28]. Here R_{1j} elements of R matrix consists of only U_{PMNS} elements.

Case	**hierarchy, Octant**	$\Delta\chi^2$	δ_{CP}	ϵ_l	$\lvert\eta_B\rvert$
1	IH, LO	25	59	7.35254×10^{-6}	3.04279×10^{-8}
2	IH, LO	25	131.5	1.00443×10^{-6}	4.15675×10^{-9}
3	IH, LO	25	246.5	3.71415×10^{-6}	1.53707×10^{-8}
4	IH, LO	25	311	3.74283×10^{-7}	1.54894×10^{-9}
5	IH, LO	16	42	-7.26506×10^{-6}	3.00659×10^{-8}
6	IH, LO	16	140.5	7.91014×10^{-6}	3.27355×10^{-8}
7	IH, LO	16	225.5	8.74966×10^{-7}	3.62098×10^{-9}
8	IH, LO	16	320.5	8.74965×10^{-7}	3.62097×10^{-9}
9	IH, HO	16	45	-1.88492×10^{-6}	7.80058×10^{-9}
10	IH, HO	16	139	-2.36693×10^{-7}	9.79536×10^{-10}
11	IH, HO	16	226.5	-7.81644×10^{-7}	3.23477×10^{-9}
12	IH, HO	16	319	-3.88288×10^{-6}	1.6069×10^{-8}
13	IH, HO	25	72	1.40342×10^{-7}	5.80793×10^{-10}
14	IH, HO	25	123	-3.73584×10^{-6}	1.54604×10^{-8}
15	IH, HO	25	257.5	1.48671×10^{-7}	6.15262×10^{-10}
16	IH, HO	25	302	-7.71976×10^{-7}	3.19476×10^{-9}

Table XI: Same as in Table IX, but IH is used.

In fig. 5 we showed variations of η_B with θ_{13}, taking range of θ_{13} within 3σ values of its best fit values, for the five favoured cases and find that values of θ_{13} around 9.0974^0 to 9.12^0 (which agrees well with the current fit data [28]) are favoured as far as matching with the best fit values of $|\eta_B|$ are concerned.

We also calculated values of Jarkslog invariant J_{CP} for these five cases, and found that they lie within present experimental limits (shown in Table XIII). Variation of J_{CP} with θ_{13}, taking range of θ_{13} within its 3σ values of its best fit values was also considered (Fig. 6), and find that J_{CP} lies within its experimental limits for these five cases even when variation of θ_{13} is taken. These results could be important, as the quadrant of leptoniv CPV phase, and octant of atmospheric mixing angle θ_{23} are yet not fixed experimentally. Also, they are significant in context of precision measurements of neutrino oscillation parameters, specially the leptonic CPV phase, Δm^2_{31} and the reactor

angle θ_{13}.

It may be noted that out of the five cases found favourable in our work here, one of the values $\delta_{CP} = 1.43\pi$ matches with the latest global fit value, $\delta_{CP} = 1.4\ \pi$. Future experiments like DUNE/LBNEs and Hyper-Kamionande [52] that would measure δ_{CP} (especially probing leptonic CPV) will support/disfavour the results presented in this work.

Acknowledgments

GG would like to thank UGC, India, for providing RFSMS fellowship to her, during which part of this work was done. DD thanks HRI, Allahabad, India for providing a postdoctoral fellowship to him. KB thanks DST-SERB, Govt of India, for financial support through a project.

Case	**hierarchy, Octant**	$\Delta\chi^2$	δ_{CP}	ϵ_l	$\lvert\eta_B\rvert$
1	IH, LO	25	59	-4.11136×10^{-6}	1.70145×10^{-8}
2	IH, LO	25	131.5	-3.26348×10^{-6}	1.35057×10^{-8}
3	IH, LO	25	246.5	9.54714×10^{-7}	3.95101×10^{-9}
4	IH, LO	25	311	1.47958×10^{-7}	6.12311×10^{-10}
5	IH, LO	16	42	3.06981×10^{-6}	1.27042×10^{-8}
6	IH, LO	16	140.5	4.12475×10^{-6}	1.707×10^{-8}
7	IH, LO	16	225.5	4.11818×10^{-6}	1.70428×10^{-8}
8	IH, LO	16	320.5	-4.80846×10^{-7}	1.98994×10^{-9}
9	IH, HO	16	45	3.74039×10^{-6}	1.54905×10^{-8}
10	IH, HO	16	139	4.18492×10^{-7}	1.73189×10^{-8}
11	IH, HO	16	226.5	2.40081×10^{-6}	9.93556×10^{-9}
12	IH, HO	16	319	-1.06298×10^{-6}	4.39907×10^{-9}
13	IH, HO	25	72	-9.54837×10^{-7}	3.95152×10^{-9}
14	IH, HO	25	123	3.41971×10^{-6}	1.91552×10^{-8}
15	IH, HO	25	257.5	1.81927×10^{-6}	7.52892×10^{-9}
16	IH, HO	25	302	3.04466×10^{-6}	1.26001×10^{-8}

Table XII: Same as in Table X but IH is used.

Serial No.	δ_{CP}**, hierarchy, octant,** J_{CP} **of our calculation**	**Quadrant Of** δ_{CP}
1.	$\delta_{CP} = 1.43\pi$, IH, HO, J_{CP} = -.03439461	third quadrant
2.	$\delta_{CP} = 1.727\pi$, IH, LO, J_{CP} = -.026588173	fourth quadrant
3.	$\delta_{CP} = 0.5277\pi$, IH, HO, J_{CP} = .035095635	second quadrant
4.	$\delta_{CP} = 0.488\pi$, IH, LO, J_{CP} = .035208214	first quadarnt
5.	$\delta_{CP} = 0.383\pi$, IH, HO, J_{CP} = .032889754	first quadrant

Table XIII: Preferred cases of δ_{CP}, octant, hierarchy and J_{CP} allowed by present range of η_B, $5.7 \times 10^{-10} < \eta_B < 6.7 \times 10^{-10}$

References

[1] G. Fogli, E. Lisi, A. Marrone, D. Montanino, A. Palazzo, et al., Phys. Rev. **D86**, 013012 (2012). arXiv:1205.5254 [hep-ph]

[2] D. Forero, M. Tortola, and J. Valle, Phys Rev. **D86**, 073012 (2012). arXiv:1205.4018 [hep-ph]

[3] M. Gonzalez-Garcia, M. Maltoni, J. Salvado, and T. Schwetz, JHEP 1212, 123 (2012). arXiv:1209.3023 [hep-ph]

[4] Debajyoti Dutta, Kalpana Bora, Mod. Phys. Lett. **A30**(07), 1550017, (2015). arXiv:1409.8248

[5] Monojit Ghosh, Pomita Ghoshal, Srubabati Goswami, Sushant K. Raut, Nucl. Phys. **B884**, 274-304 (2014). arXiv:1401.7243

[6] I. Girardi, S. T. Petcov, A.V. Titov, Eur. Phys. J. **C75**(7), 345 (2015). arXiv:1504.00658.

[7] Sin Kyu Kang, M Tanimoto, Phys. Rev. **D91**(7), 073010 (2015). arXiv:1411.3104.

[8] LHCb Collaboration (Roel Aaij (NIKHEF, Amsterdam) et al.) Phys. Rev. Lett. **114**, 041801, 4 (2015), arXiv:1504.00658. LHCB-PAPER-2014-059, CERN-PH-EP-2014-271, LHCB-PAPER-2014-059-AND-CERN-PH-EP-2014-271

[9] Patrick Huber, Manfred Lindner, Thomas Schwetz, Walter Winter, JHEP **0911** 044 (2009). arXiv:0907.1896

[10] Kalpana Bora, Debajyoti Dutta, Pomita Ghoshal, Mod. Phys. Lett. **A30**(14), 1550066, (2015). arXiv:1405.7482

[11] M. C. Gonzalez-Garcia, M. Maltoni, A. Yu. Smirnov, Phys. Rev. **D70**, 093005 (2004). hep-ph/0408170

[12] Animesh Chatterjee, Pomita Ghoshal, Srubabati Goswami, Sushant K.Raut, JHEP **1306**, 010(2013). arXiv:1302.1370

[13] Sandhya Choubey, Anushree Ghosh, JHEP 1311, 166 (2013). arXiv:1309.5760

[14] Daljeet Kaur, Naimuddin, Sanjeev Kumar, Eur. Phys. J. **C75**(4), 156(2014). arXiv:1302.1370

[15] LBNE Collaboration, C. Adams et al., arXiv:1307.7335.

[16] T. Akiri et al. [LBNE Collaboration], arXiv:1110.6249 [hep- ex]

[17] NOνA Collaboration, D. Ayres et al., hep-ex/0503053.

[18] T2K Collaboration, K. Abe et al., Phys. Rev. Lett. **107**, 041801 (2011). arXiv:1106.2822

[19] MINOS Collaboration, P. Adamson et al., Phys. Rev. Lett. **107** 181802 (2011). arXiv:1108.0015

[20] D. Autiero, J. Aysto, A. Badertscher, L. B. Bezrukov, J. Bouchez, et al., JCAP **0711**, 011 (2007). arXiv:0705.0116

[21] G. C. Branco, R. G. Felipe and F. R. Joaquim, Rev. Mod. Phys. **84**, 515 (2012). arXiv:1111.5332 [hep-ph].

[22] F. P. An et al. [Daya Bay Collaboration], Phys. Rev. Lett, **108**, 171803 (2012); Chin. Phys.C **37**, 011001 (2013), arXiv:1210.6327 [hep-ex]; J. K. Ahn et al. [RENO Collaboration], Phys. Rev. Lett. **108**, 191802 (2012). arXiv:1204.0626 [hep-ex]; Y. Abe et al. [Double Chooz Collaboration] Phys. Rev. Lett., **108**, 131801 (2012).

[23] B. Pontecorvo. Sov. Phys. JETP, 6, 429, 1957 ; Sov. Phys. JETP, 26, 984, (1968) ; Z. Maki, M. Nakagawa and S. Sakata, Prog. Theor. Phys., 28, 870 (1962).

[24] F. Capozzi, G.L. Fogli, E. Lisi, A. Marrone, D. Montanino, A. Palazzo , Phys. Rev. **D89**, 093018 (2014), arXiv:1312.2878 [hep-ph]; G. L. Fogli, E. Lisi, A. Marrone, D. Montanino, A. Palazzo and A. M. Rotunno, Phys. Rev. **D 86**, 013012 (2012), arXiv:1205.5254 [hep-ph]; D. V. Forero, M. Tortola and J. W. F. Valle, Phys. Rev. D 90 (2014), arXiv:1405.7540 [hep-ph].

[25] M. C. Gonzalez-Garcia, M. Maltoni and T. Schwetz, JHEP **1411**, 052 (2014), arXiv:1409.5439 [hep-ph].

[26] V. Barger, D. Marfatia, and K. Whisnant, Phys. Rev. **D66**, 053007 hep-ph/0206038.

[27] H. Minakata and H. Nunokawa, JHEP **0110**, 001 (2001). hep-ph/0108085

[28] K. A. Olive et al. [Particle Data Group Collaboration], Chin. Phys. **C 38**, 090001 (2014); D. V. Forero, M. Tortola and J. W. F. Valle, Neutrino oscillations refitted, Phys. Rev. **D 90** (2014) 093006, [1405.7540]; G.L. Fogli, E. Lisi, A. Marrone, D. Montanino, A. Palazzo, and A.M. Rotunno, Phys. Rev. **D 86**, 013012 (2012); M.C. Gonzalez-Garcia, M. Maltoni, J. Salvado, and T. Schwetz, JHEP 1212, 123 (2012); F. Capozzi, G. L. Fogli, E. Lisi, A. Marrone, D. Montanino and A.

Palazzo, arXiv:1312.2878 [hep-ph].

[29] W. Buchmuller, P. Di Bari (DESY), M. Plumacher, Nucl.Phys. B**643**, 367-390 (2002), Nucl.Phys. B**793**, 362 (2008), hep-ph/0205349

[30] R.N. Mohapatra, Hai-Bo Yu, Phys.Lett. **B644**, 346-351 (2007), hep-ph/0610023

[31] S. Bhupal Dev. talk presented at DAE HEP symposium, IITG, Dec 8-12, 2014.

[32] P.S. Bhupal Dev, Chang-Hun Lee, R.N. Mohapatra, J. Phys. Conf. Ser. **631**1, 012007 (2015)

[33] Gayatri Ghosh, Kalpana Bora, talk presented at DAE HEP symposium, IITG, Dec 8-12, 2014, Springer Proc. Phys. **174** (2016) 287-291.

[34] Z. Maki, M. Nakagawa and S. Sakata, Prog. Theor. Phys. **28**, 870 (1962).

[35] Narendra Sahu, S.Uma Sankar, Phys.Rev. **D71**, 013006 (2005), hep-ph/0406065

[36] M. Fukugita and T. Yanagida, Phys. Lett. **B17**4, 45 (1986).

[37] R. N. Mohapatra and X. Zhang; Phys. Rev. **D46**, 5331 (1992).

[38] M. Plumacher, Z. Phys. **74**, 549 (1997).

[39] S. Davidson and A. Ibarra, Phys. Lett. **B 535**, 25 (2002). arXiv: hep-ph/0202239

[40] R. N. Mohapatra, S. Nasri, Hai-Bo Yu, Phys.Lett. **B615**, 231-239 (2005). hep-ph/0502026

[41] J.A. Casas and A. Ibarra, Nucl. Phys. B618, 171-204 (2001)hep-ph/0103065

[42] Kalpana Bora, Gayatri Ghosh, J. Phys. Conf. Ser., **481**, 012016 (2014).

[43] Kalpana Bora, Debajyoti Dutta, Pomita Ghoshal, JHEP **12**, 025 (2012). arXiv:1206.2172

[44] Kalpana Bora, Gayatri Ghosh, Eur. Phys. J. C**75**, (2015) 9, 428, arXiv:1410.1265

[45] G. t Hooft, Phys. Rev. Lett **37**, 8 (1976)

[46] F. R. Klinkhamer, N. S. Manton, Phys. Rev. D **30**, 2212 (1984)

[47] V. A. Kuzmin, V. A. Rubakov, M.E shaposhikov, Phys Lett B **155**, 36 (1985)

[48] S. Yu Khlebnikov, M.E Shaposhnikov, Nucl phys B **3D8**, 885 (1968)

[49] F. Buccella, D. Falcone, F. Tramontano, Physics Letters B **524** 241244 (2002).hep-ph/0108172

[50] B. D. Fields, P. Molarto and S. Sarkar, "Big Bang Nucleosynthesis," in Review of PDG-2014 (Astrophysical Constants and Parameters)

[51] Anjan S. Joshipura, Ketan M. Patel, Phys. Rev. **D83**, 095002(2011), arXiv:1102.5148

[52] Matthew Malek, talk presented at 17th Lomonoscov Conference on Elementary Particle Physics, Moscow State University-26 August 2015.